X-ray diffraction measurements of Mo melting to 119 GPa and the high pressure phase diagram

D. Santamaría-Pérez,[1,a)] M. Ross,[2,b)] D. Errandonea,[3] G. D. Mukherjee,[1] M. Mezouar,[4] and R. Boehler[1]
[1]*Max-Planck Institute für Chemie, Postfach 3060, D-55020 Mainz, Germany*
[2]*Lawrence Livermore National Laboratory, Livermore, California 94551, USA*
[3]*Dpto. Fís. Apl.-ICMUV, Fund. General de la Univ. de Valencia, C/Dr.Moliner 50, 46100 Burjassot, Spain*
[4]*ESRF, 6 Rue Jules Horowitz, BP 220, 38043 Grenoble Cedex, France*

(Received 25 November 2008; accepted 27 January 2009; published online 25 March 2009)

In this paper, we report angle-dispersive X-ray diffraction data of molybdenum melting, measured in a double-sided laser-heated diamond-anvil cell up to a pressure of 119 GPa and temperatures up to 3400 K. The new melting temperatures are in excellent agreement with earlier measurements up to 90 GPa that relied on optical observations of melting and in strong contrast to most theoretical estimates. The X-ray measurements show that the solid melts from the bcc structure throughout the reported pressure range and provide no evidence for a high temperature transition from bcc to a close-packed structure, or to any other crystalline structure. This observation contradicts earlier interpretations of shock data arguing for such a transition. Instead, the values for the Poisson ratios of shock compressed Mo, obtained from the sound speed measurements, and the present X-ray evidence of loss of long-range order suggest that the 210 GPa (~4100 K) transition in the shock experiment is from the bcc structure to a new, highly viscous, structured melt. © *2009 American Institute of Physics*. [DOI: 10.1063/1.3082030]

I. INTRODUCTION

The phase diagram of molybdenum has become a controversial topic as the result of conflicting interpretations of shockwave melting measurements,[1] laser-heated diamond-anvil cell (DAC)[2(a),2(b),3,4] melting, theory, and computer simulations.[5–8] For example, the relevant data for Mo, taken from the references,[1,2(a),8] are plotted in Fig. 1 showing the discrepancy between most of the theoretical melting curves and the shock wave and DAC melting experiments. Chronologically, the narrative begins with shock experiments for Mo, made in 1989 by Hixson *et al.*,[1] in which two discontinuities in the longitudinal sound speed were detected. One discontinuity is near 210 GPa (~4100 K), and a second near 390 GPa (~10 000 K). The first discontinuity has been interpreted as a bcc-hcp transition, and the second as hcp melting. While the pressures are measured, temperatures are calculated due to experimental limitations. Since the calculated temperatures vary by more than 30% with theoretical models, for consistency we employ the temperatures first reported by Hixson *et al.*[1] Subsequently, the Mo melting curve was measured statically in a DAC to 90 GPa (3180 K), by heating the sample and observing a continuous speckled motion in the liquid[2(a)] and equally important, by the observation of distinct textural melt features [see Fig. 1 in Ref. 2(a)]. According to the DAC measurements, the low Mo melting slope extrapolates to the first shock discontinuity near 210 GPa rather than the 390 GPa discontinuity. This caused some debate since the 210 GPa point had been interpreted as a bcc-hcp transition. Because doubts have been raised regarding optical methods to detect melting in the DAC, we performed new experiments where melting is detected by X-ray diffraction.

In Sec. II of this paper, we report new angle-dispersive X-ray diffraction data of molybdenum melting, measured in a double-sided laser-heated DAC up to a pressure of 119 GPa and temperatures up to 3400 K. The observation of diffusive scattering in the X-ray patterns and the subsequent recrystallization upon quenching confirm the earlier measurements that relied on optical observations of the melt. The X-ray measurements provide no evidence for a high temperature transition from bcc to a close-packed structure or any other crystalline structure. It should be pointed out that for most

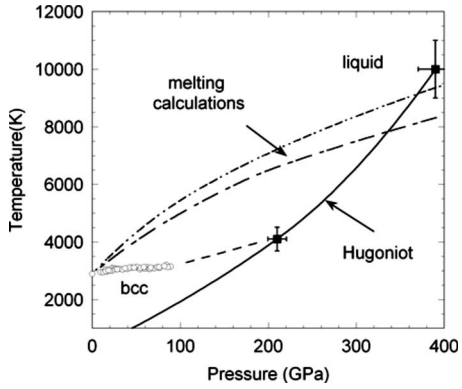

FIG. 1. Mo melting and shock transition data. DAC melting, open circles (Ref. 4) extended to 210 GPa (small dashed line). Shock transitions (crosses) (Ref. 1) and calculated Hugoniot (solid curve) (Ref. 8). Calculated melting curves of Ref. 5(dashed-dotted), and Ref. 6 (long dashes).

a)Electronic mail: santa@mpch-mainz.mpg.de.
b)Electronic mail: marvinross@earthlink.net.

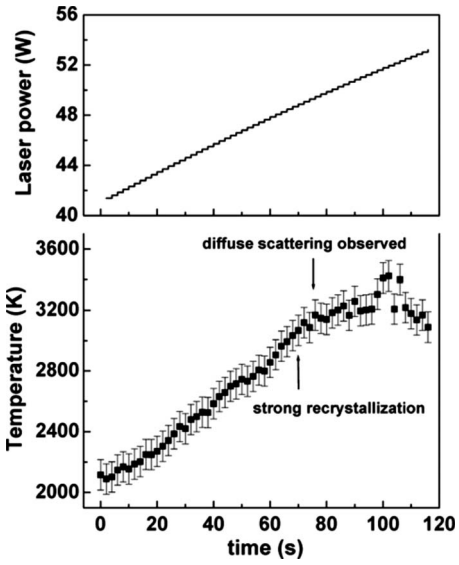

FIG. 2. Evolution of the Mo sample temperature at 81 GPa (89 GPa after P_{th} consideration) with increasing laser power. At temperatures of about 150 K below melting (appearance of diffuse x-ray scattering), rapid changes in the position and intensity of the Mo peaks (recrystallization) were observed. The melting temperature was taken at the onset of the diffuse scattering. From this point, temperatures rise slower with increasing laser power and fluctuate.

materials studied in the laser-heated diamond cell, optical methods to detect melting have shown excellent agreement in the melting temperatures with accurate low pressure measurements, shock experiments and theory (alkali halides,[9,10] metals,[11–16] etc.). In Sec. III, we report values for the Poisson ratios of shock compressed Mo, obtained from the sound speed measurements of Hixson *et al.*,[1] that provide evidence that the 210 GPa (~4100 K) transition is from the bcc to a noncrystalline state, and cannot be a bcc-hcp transition as proposed. In fact, the Poisson ratios strongly suggest that the 210 GPa transition is an extension of the diamond-anvil melting measurements. Both the new DAC experiments and the reanalysis of the shock data provide new insight into the high pressure phase diagram of this Mo.

Unusually low melting slopes have now been found in all seven of the early transition metals studied,[2(a)] Mo, Ta, W, Cr, Ti, V, and Y, indicating that the measurements for Mo are not unique, but are characteristic of this class of metals. The origin of these low melting temperatures has been attributed to the presence in the liquid of tetrahedral and icosahedral structures with short range order (ISRO).[3] In Sec. IV we employ a free energy model that explains thermodynamically how the local structures lower the melting temperatures and influence the Mo phase diagram.

II. X-RAY DIFFRACTION MEASUREMENTS

The X-ray measurement data reported here are from five different runs. Disks or grains of molybdenum with 99.99% purity (Aldrich, Prod. Nr. 366986), 15–25 μm in diameter, and 10 μm thickness were loaded into a new type diamond cell ("plate DAC") with conical anvils (280 μm culet size) with an X-ray aperture of 50°.[17] The samples were placed in the approximate center of a 100 μm diameter hole of a tungsten gasket that was preindented to a thickness of 30 μm. Al_2O_3, KCl, or $MgSiO_3$ dry gel were used as pressure transmitting media and to thermally insulate the sample from the diamonds. In one experiment the sample assemblage con-

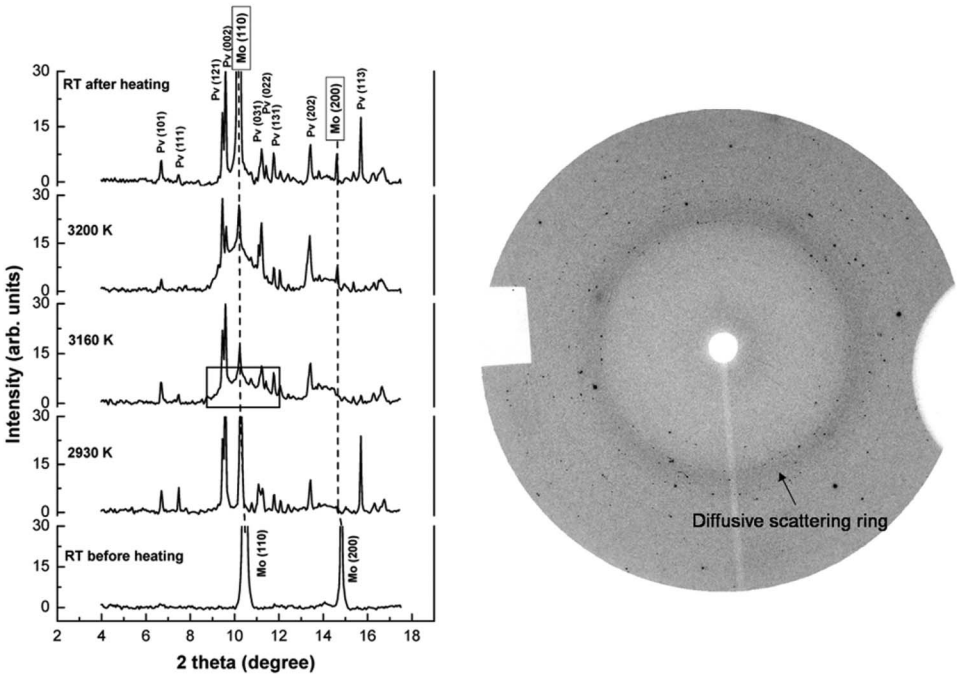

FIG. 3. (a) X-ray diffraction patterns of the same molybdenum sample at 89 GPa (pressure before heating 109 GPa). The pressure medium was $MgSiO_3$ dry gel. At 3160 K, a significant decrease in the intensity of the diffraction peaks of bcc-Mo and the appearance of the diffusive halo associated to liquid molybdenum is observed (see box). The reason for the coexistence of crystalline and liquid phases is most likely temperature fluctuations in the molten sample due to changes in the laser absorption. All the peaks of the diffraction patterns collected before, during, and after heating correspond to bcc-Mo and the $MgSiO_3$ perovskite phase. (b) CCD image of the x-ray pattern of the same sample at 3200 K showing diffuse scattering.

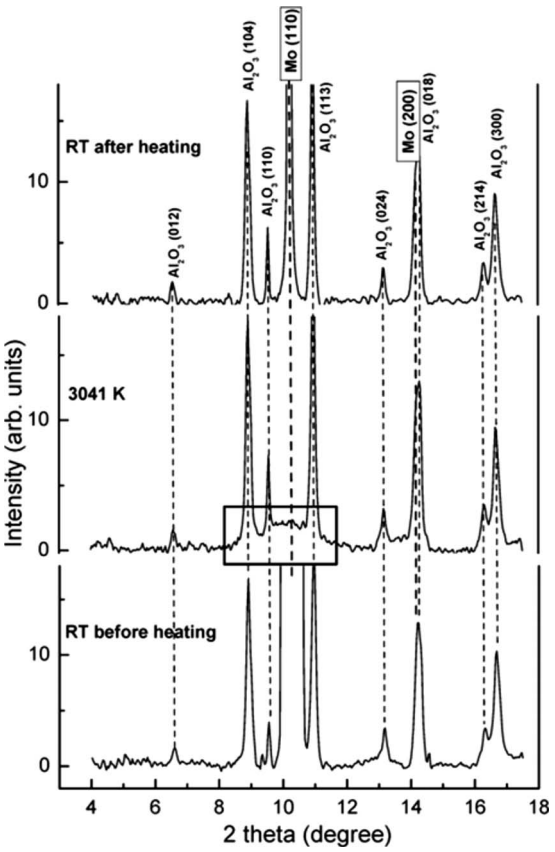

FIG. 4. X-ray patterns of the Mo sample at 63 GPa (71 GPa after P_{th} consideration). The pressure medium was Al_2O_3. At 3041 K, the bcc-Mo peaks disappear completely and a diffuse scattering halo characteristic of melting becomes visible (see box). After heating, the Mo peaks reappear. All the peaks of the diffraction patterns correspond to bcc-Mo and Al_2O_3, indicating that no chemical reaction between the molten sample and pressure medium had occurred.

sisted of two single crystal plates of Al_2O_3 and a ruby plate with 10 μm thickness each. The center Al_2O_3 plate had a hole with 20 μm in diameter that contained the sample. For three runs, a 15–20 μm Mo grain was embedded in dry, powdered $MgSiO_3$ gel, and in one run a Mo grain was embedded in KCl powder. All starting materials were dried under vacuum at 120 °C and then flushed with argon prior to pressurizing. In the runs without a ruby plate, small ruby chips were placed close to the sample. Pressures were measured before and after heating by the ruby fluorescence method.[18] The pressures measured in this way were in good agreement with those obtained from the equation of state (EOS) of Mo,[19,20] Al_2O_3,[21] and $MgSiO_3$-perovskite,[22] which formed at high P-T conditions from the gel.

The samples were heated from both sides with two 40 W Nd:YVO_4 infrared lasers ($\lambda = 1.064$ μm). The laser beams were defocused to create a hotspot of 15–20 μm diameter. The power and focusing of both lasers was adjusted to minimize the difference of temperatures between both sides of the sample to 100 K. Temperatures were measured from the center of the hotspot from areas of 2 μm diameter by fitting Planck's radiation function to the spectra in the spectral range of 600–800 nm assuming wavelength-independent emissivities.[23] Temperature gradients in the center of the hotspot were within 100 K in an area with 10 μm in diameter. During temperature cycling, slight changes in the location of the hotspot and alignment were corrected by piezoelectric mirror stages in order to maintain the center of the hotspot on the pinhole of the spectrometer.

The thermal signals emitted by the sample were collected from both sides by Schwarzschild reflecting objectives, which also serve as imaging optics. On the side of the incident X-ray beam a 45° mirror with a 2 mm hole was used to simultaneously collect X-ray patterns and measure temperatures. On the back side, a 45° mirror mounted on a fast pneumatic translation stage allowed the collection of the emitted light in between X-ray exposures. X-ray measurements were performed at the ID-27 beamline of the European Synchrotron Radiation Facility (ESRF) using an X-ray wavelength of 0.3738 Å and a beam diameter of 3 μm (full width at half maximum). Diffraction images were recorded every 2 s with a Mar345 charge coupled device (CCD) detector while the power of the lasers was increased in small steps. The method of rapid X-ray detection has been previously used for Pb (Ref. 24) and for iron,[25] and also for low Z elements such as oxygen.[26] For iron and oxygen, the results are in good agreement with optically detected melting data. The diffraction patterns from the CCD detector were integrated as a function of 2θ in order to obtain one-dimensional diffraction profiles. The indexing and refinement of the powder patterns were performed using the DICVOL (Ref. 27) and POWDERCELL (Ref. 28) program packages. All the peaks of the diffraction patterns collected before, during and after the heating process correspond to bcc-Mo and the pressure transmitting media.

The detection of melting by X-ray diffraction at very high pressure is not straightforward because the intensity of diffuse scattering from a liquid is relatively low. A diffusive scattering halo can only be observed if a large portion of the sample probed by X-rays is molten. However, this is difficult to achieve because during melting the absorption properties of the sample change rapidly. Moreover, sample containment (to avoid the dispersion of the molten sample) and perfect alignment of X-ray beam and hotspot are essential. Nevertheless, in three runs (out of five) we managed to observe typical changes in the diffraction patterns related to melting such as diffuse scattering rings and the disappearance or significant decrease in the intensity of the X-ray diffraction peaks of the solid. In the other two runs, using polycrystalline KCl and $MgSiO_3$ dry gel as pressure media, no diffuse scattering halo was observed. In these two and all the other runs, however, we observed fast changes in the position and intensity of the diffraction spots, which is indicative of the onset of melting (see below).

Figure 2 shows the evolution of the temperatures of the sample with increasing laser power. The initial temperature of the ramp was 2200 K, far below the melting temperature of molybdenum. At this temperature the initially fine-grained polycrystalline sample was already strongly recrystallized as evident from the spotty diffraction patterns. The powers of the lasers were then increased to produce small temperature steps of about 30 K. At melting (at a temperature of 3160 K at 89 GPa; Fig. 2) we observed diffusive scattering and a

TABLE I. Melting temperatures of molybdenum, measured in the laser-heated diamond cell at different run conditions.

Pressure after heating (GPa)	Pressure at melting, including P_{th} (GPa)	Pressure medium	Melting temperature (K)	Melting detection criterion (see text)
47 ± 1	55 ± 2	KCl	2990 ± 80	Rapid recrystallization
63 ± 1	71 ± 2	Al_2O_3	3041 ± 100	Diffusive scattering and complete disappearance of bcc-Mo diffraction peaks
81 ± 1	89 ± 2	$MgSiO_3$	3160 ± 120	Diffusive scattering
110 ± 1	117 ± 2	$MgSiO_3$	3140 ± 120	Rapid recrystallization
111 ± 1	119 ± 2	$MgSiO_3$	3302 ± 140	Diffusive scattering

significant decrease in the intensity of the diffraction peaks of molybdenum [see Figs. 3(a) and (b)] or their complete disappearance (see Fig. 4).

Rapid recording of X-ray patterns during temperature cycling provided valuable information: raising temperatures from about 2200 K did not noticeably change the diffraction patterns. However about 150 K below the appearance of diffusive scattering or the disappearance of the Mo peaks we always observed rapid changes in the position and intensity of the diffraction spots in the diffraction patterns: typically a decrease in the number of spots and an increase in their intensity. This abrupt change in the diffraction patterns must be due to the onset of melting of the sample allowing rapid growth and reorientation of grains in the polycrystalline sample. Subsequently, at slightly higher temperatures, a diffuse scattering halo became visible [see Figs. 3(a) and (b)]. This halo is a consequence of the loss of atomic local order, which it is attributed to the fact that the sample was molten. In Fig. 3(a), a significant decrease of the intensity of the peaks of bcc-Mo was observed, but they are still present. These peaks correspond to crystalline Mo that coexists with the liquid phase. The reasons for this apparent coexistence are most likely fast temperature fluctuations in the molten sample due to local changes in the laser absorption. The X-ray exposure was about 2 s, thus sampling both solid and liquid states. The melting temperature was taken at the onset of diffuse scattering but, in fact, the melting temperature may be slightly lower (onset of melting) and the fact that the temperature is measured from the hottest portion of the sample (heated surface).

Typically, at the onset of melting, the temperature increase becomes smaller with increasing laser power (see Fig. 2). This observation is most likely due to a lower absorption of the laser radiation by the melt than by the solid and an increasing melt fraction at increasing laser power. This discontinuity in the temperature rise has often been used to determine melting temperatures in laser-heating diamond cell experiments.

When the laser power was decreased, the bcc-Mo diffraction spots reappeared at the same time as the diffuse scattering disappeared, indicating freezing of the sample. The fact that only Mo diffractions were observed showed that chemical reaction between molten molybdenum and the pressure transmitting medium had not occurred. Visual observations of the samples after heating showed typical melt textures.

The melting data reported here were taken at pressures of 47, 63, 81, 110, and 111 GPa. Pressures were measured after heating using the ruby fluorescence scale, the EOS of Mo and the EOS of the pressure transmitting media. For these three methods, the pressures were within 1 GPa. To these pressures, we have to add the thermal pressure consequence of heating the sample. The thermal pressures were estimated calculating an approximate volumetric thermal expansivity (Ref. 29) and, as the volume of Mo did not change significantly with temperature, we assume that the bulk modulus only depends on pressure ($K_P = K_0 + K_0'^* P$). Thus, the thermal pressure was determined: $P_{th} = \alpha^* K_P^* T$, with values between 7 and 8 GPa at melting temperatures in the five runs. Therefore, the pressures at melting were 55, 71, 89, 117, and 119 GPa, respectively. The run conditions, the melting temperatures and the criteria used to detect melting are listed in Table I. In the runs at 47 and 63 GPa, using KCl and single crystal Al_2O_3 plates, respectively, as a pressure transmitting medium, no substantial change in pressure after a heating cycle was observed with respect to that measured before heating. In the runs at 81, 110, and 111 GPa with $MgSiO_3$ dry gel as pressure transmitting medium, a significant pressure release (about 25 GPa) was detected after heating. This pressure difference is due to the formation of crystalline $MgSiO_3$-perovskite, which is significantly denser than the amorphous starting material.

At 63, 81, and 111 GPa (71, 89, and 119 GPa, respectively, after adding the thermal pressure), we observe diffuse scattering from liquid Mo. Melting temperatures for these three experiments were 3041, 3160, and 3302 K, respectively. At these pressures, the melting temperatures of Al_2O_3 and $MgSiO_3$ are substantially higher,[30,31] and therefore melting of the pressure media could not have contributed to the observed diffuse scattering. In the two other experiments, no diffuse scattering but the onset of rapid recrystallization was observed at 2990 K and 47 GPa (55 GPa after P_{th} consideration) and at 3140 K and 110 GPa (117 GPa after P_{th} consideration). As mentioned above, these recrystallization temperatures (assigned to partial melting) are typically lower than those obtained from observation of diffusive scattering. Our data on Mo are represented in Fig. 5 together with pre-

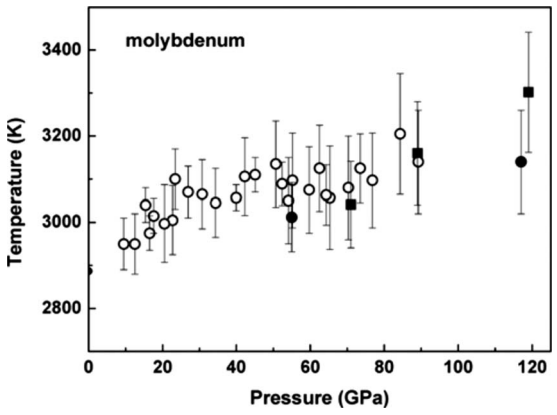

FIG. 5. DAC melting data of Mo. Previous measurements using the laser speckle method and melt textures to detect melting are represented by empty circles (Ref. 2(a)). Present X-ray diffraction data are represented by solid squares: fully melted (diffuse scattering) and by solid circles: partially melted (recrystallization).

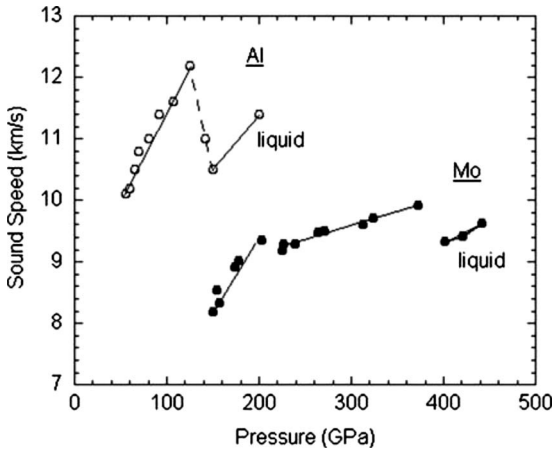

FIG. 6. Longitudinal and bulk sound velocities obtained from shock experiments for Al (Ref. 33) and Mo (Ref. 1).

vious static compression results where melting was determined by the laser speckle method.[2(a)] Our data are consistent with these earlier optical measurements and show that the melting temperatures level off at 3300 K and 119 GPa. They not only confirm the earlier DAC melting data but also rule out the possibility of a solid-solid high-pressure high-temperature (HP-HT) phase transition. A re-evaluation of earlier Poisson ratio data from shock experiments described in the following paragraph will improve our knowledge on the HP-HT structural behavior of Mo.

III. POISSON RATIOS AND SHOCK SOUND SPEED MEASUREMENTS

The Poisson ratio (ν) is the ratio of strain in the lateral direction, relative to the strain in the longitudinal direction. It can be calculated from the longitudinal (C_L) and bulk (C_B) sound speeds measured in shock experiments[1] by using the expression

$$C_L/C_B = [3(1-\nu)/(1+\nu)]^{1/2}.$$

In the present application, the Poisson ratios provide useful criteria for examining the structural changes in Mo along the Hugoniot. For isotropic materials, such as ideal bcc and close-packed structures such as hcp and fcc, $\nu=0.25$, and for liquids $\nu=0.5$. For Mo, $\nu=0.31$, and for Al, $\nu=0.32$. For most close-packed metals ν is in the range of 0.28–0.36. For the purpose of this study we refer to any phase of Mo with a value of ν above this range, as non-close packed. Our use of this term necessarily includes phases such as glasses, amorphous solids, etc., that may be present, but are beyond our ability to designate.

In order to acquire some guidance in interpreting the Mo data, we first consider the sound speed measurements of Shaner *et al.*[32] that lead to the detecting shock melting of Al. Al melting has been measured in a DAC,[33] and it is understood to be a transition directly from an fcc solid to a pure atomic-like liquid.[34] Plotted in Fig. 6, are the sound speed measurements of shock compressed Al and Mo (Ref. 1) versus the Hugoniot pressure. The sound speeds for fcc Al, increase linearly with pressure up to 120 GPa and then show a discontinuous drop to the liquid caused by the loss of shear strength. A data point has been taken in the mixed phase region at 145 GPa is indicative of a mixed solid-liquid phase. The Poisson ratios calculated for Al are plotted in Fig. 7. In the fcc phase, they show a small increase in the Ratio from $\nu=0.32$ at $P=0$, to $\nu=0.34$ near 120 GPa. This is followed by a discontinuous jump (melting) to the liquid value of $\nu=0.5$. The singular experimental point at 140 GPa, and $\nu=0.46$, lies in the mixed phase region.

In the case of Mo, an interpretation of the sound speed data is problematical. The values of ν obtained from the reported Mo sound speeds[1] are plotted in Fig. 8. Noteworthy is the absence of shock measurements below 150 GPa. A similar plot can be constructed for Ta.[32] Following the example of Al we assume the $P=0$ GPa bcc value of $\nu=0.31$, remains a constant up to 119 GPa, the highest pressure at which Mo DAC melting measurements had been made. The value of ν then increases to $\nu=0.42$ near 150 GPa that is the lowest pressure at which shock measurements were made. This means that none of the shock measurements made for Mo were in the bcc phase. Clearly then, there must be a bcc to noncrystalline transition starting at some pressure between 119 and 150 GPa (~3000 K). This would place the shock transition in agreement with a linear extrapolation of the DAC melting curve.

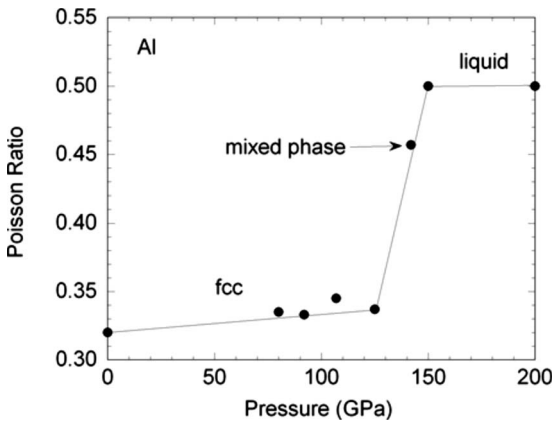

FIG. 7. Poisson ratios for Al vs pressure, obtained from the longitudinal and bulk sound velocities obtained from shock experiment (Ref. 33).

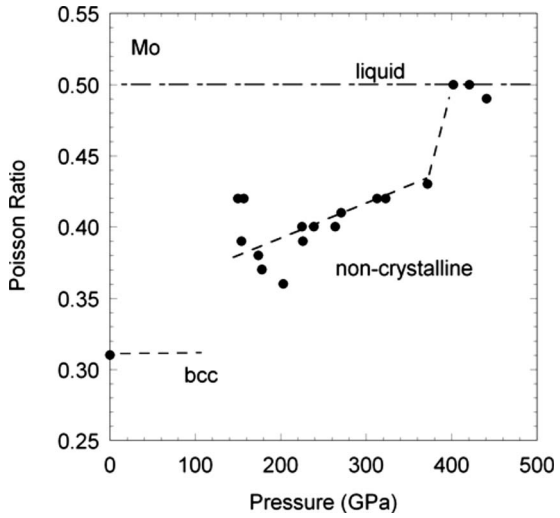

FIG. 8. Poisson ratios for Mo vs pressure, obtained from the longitudinal and bulk sound velocities obtained from shock experiments (Ref. 1).

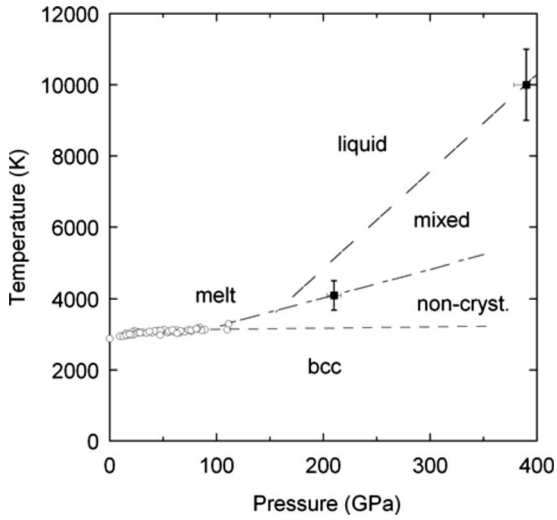

FIG. 9. The proposed Mo phase diagram described in text. DAC melting (open circles) (Ref. 4). Shock transitions (crosses) (Ref. 1). The small dashed curve is a bcc to non-close-packed solid phase line. The long dashed line is an extension of the DAC melting curve passing through the 210 GPa shock transition. The dashed-dotted line defines roughly a predicted mixed viscous melt to liquid phase line.

At pressures above 150 GPa, the values of ν decrease sharply to 210 GPa, and rise again at 220 GPa. This is the discontinuity reported as the 210 GPa shock transition, and it is not directly from the bcc phase, but it is from a structure in the intermediate pressure range from 150 to 210 GPa. Hixson *et al.*[1] noted that at 210 GPa the Poisson ratio of 0.4 was considerably higher than the normal density value. At pressures above 210 GPa the value of ν rises steadily to $\nu=0.44$ at 380 GPa, where it jumps to the liquid value of $\nu=0.5$, at 390 GPa and melts. The nearly linear increase in the Poisson ratio above 210 GPa indicates a continuous loss of shear strength. This loss is consistent with a solid-liquid mixture in which the liquid fraction is increasing as it approaches the pure liquid. While the Poisson ratios do not provide specific determinations of the atomic structures they do eliminate the possibility of a bcc-hcp, or any other crystalline phase transition, at 210 GPa.

Based on the constraints imposed by the static DAC measurements and Poisson ratios from shock experiments, we propose the phase diagram, described in Fig. 9. In this diagram the bcc phase extends at 3250 K to 150 GPa, the pressure at which the Poisson Ratios point to a transition from bcc to a new noncrystalline phase, possibly close to the A15 structure. This structure is known to compete favorably with bcc, for the neighboring metals Mo, Nb, Ta, and W.[35] The melt line extends to the 210 GPa shock discontinuity. Above 150 GPa the melt is a solid-liquid mixture bounded roughly by a transition region extending from 150 GPa (4100 K) to 390 GPa (10 000 K). This prediction can be verified by new shock measurements of the sound speeds between about 100 and 200 GPa.

IV. FREE ENERGY MODEL

In this section we will attempt to show, by the use of a free energy model, that the unique features of the Mo phase diagram are a consequence of the presence of local structures in the liquid. This model is clearly not predictive of the melting of Mo beyond the *P-T* range of this paper, but it allows to expand our understanding of the physics responsible for the low melting temperatures recorded by the experimental measurements. Evidence for the presence of local structures in transition metal liquids is supported by an extensive body of experimental and theoretical investigations.[35–43] The stability of these structures are attributed to the partially filled *d*-electron bands and directional bonding of transition metals that lead to the formation of preferred local structures with polytetrahedral, or fivefold ISRO. These structures have a lower energy, and are more densely packed than bcc, fcc, and hcp structures.

Local structures in the liquid are at the most elementary level soluble impurities that lower the melting temperature by increasing the communal entropy. This is classic freezing point depression. Since local structures are denser than the atomic liquid, compression favors an increase in their concentration with pressure thereby maintaining a melting temperature lowering and leading to low melting slopes (dT/dP). Although it is impossible to create a crystal with icosahedral symmetry, randomly packed clusters with ISROs may evolve continuously and be interconnected throughout the liquid frustrating long-range ordering and crystal formation.

While a rigorous theoretical prediction of the Mo melting curve is clearly beyond the scope of this report, a considerable degree of understanding can be acquired by employing a free energy model in which calculations of the melting curve are made, first by omitting local structures and subsequently by including the free energy contribution of the local structures. A version of the model has been described previously.[3,44]

For the first case, we write the excess Helmholtz free energy for a system of solid and liquid atoms interacting by inverse-power repulsive potentials, $\phi(r)=B/r^n$, as

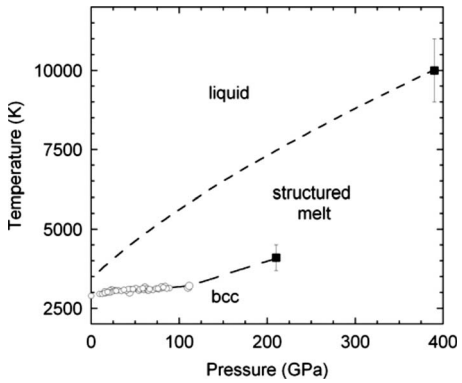

FIG. 10. Calculated model melting curves. DAC open circles (Refs. 3 and 4). Melting curves omitting local structures (small dashed curve), and including local structures by fitting to measurements (dashed-dotted). Shock transitions (crosses) (Ref. 1).

$$F_{ex}^{s} = U_M + F_{\text{th-invn}}^{s},$$
$$F_{ex}^{l} = U_M + F_{\text{th-invn}}^{l}. \tag{1}$$

In each expression, the first term is the Madelung energy (U_M) of the solid and the second is the thermal free energy of atomic motion in the solid and liquid, respectively. The thermodynamic properties of the inverse-power potential has been studied extensively by computer simulations, and the thermal free energy terms in Eq. (1) have been fitted to analytic expressions of the free energy.[45] Although the same U_M is used to represent the solid and liquid Madelung energy, the thermal contributions to the liquid free energy are determined from a fit to the total excess free energy, in effect correcting for the Madelung term. This is a reasonable approximation for transition metals, in which the volume changes of melting are typically 1%–2 %.

A useful simplification for real systems is to replace the Madelung energy, U_M, by U_{lat} the lattice energy determined from a Birch–Murnaghan fit to the experimental room temperature isotherm,[46] corrected to $T=0$ K. The excess Helmholtz free energy can now expressed written as

$$F_{ex}^{s} = U_{\text{lat}} + F_{\text{th-invn}}^{s}.$$
$$F_{ex}^{l} = U_{\text{lat}} + F_{\text{th-invn}}^{l}. \tag{2}$$

The model has the attractive feature that it reproduces the room temperature solid isotherm, and provides a thermodynamically consistent set of solid and liquid free energy functions. Melting is determined by matching free energies of the two phases.

As it stands, the model requires two adjustable parameters, B and n, in the potential. As in the bcc-hcp case we chose $n=6$, and $B=400$ eV cm^6, values that had been determined by fitting the model predictions to the experimental Mo Hugoniot.[1] Using these parameters two sets of melting calculations were made. In one set, using Eq. (2), atoms in the bcc solid melt to an atomic liquid. In the second set, terms were added to the liquid free energy in order to account for the influence local structures. In this case, the free energy of the liquid is modified to

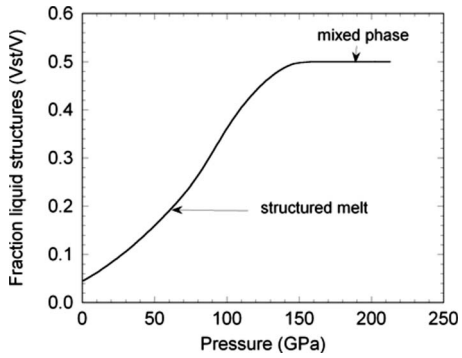

FIG. 11. Calculated volume fractions of local structures in the melt vs pressure as described in text.

$$F_{ex}^{l} = U_{\text{lat}} + F_{\text{th-inv6}}^{l} + xU_{cl}^{l} + kT[x \ln x + (1-x)\ln(1-x)]. \tag{3}$$

The added terms are U_{cl}, the binding energy of a local structure, and the communal entropy of liquid-cluster mixing. Since U_{cl} is unknown, and to avoid adding poorly known parameters we set $U_{cl}=0$. The parameter x is defined here as the volume fraction of local structures in the melt, $x=V_{\text{st}}/V$, where V_{st} is the effective total volume of local structures in a volume, V. The volume fraction, x, is used here as a parameter to fit the DAC melting measurements and the 210 GPa shock discontinuity. By adjusting value of x to fit the measurements it implicitly includes contributions from the omitted U_{cl} and geometric frustration that is not a thermodynamic driver, but does act to inhibit long-ranged order and crystalline formation. Figure 10 shows the DAC melting measurements, the shock melting points, and calculations made with the present model of melting, without local structures and with local structures fitted to the DAC and 210 GPa shock discontinuity. The melting curve calculated by omitting local structures is in very good agreement with the computer simulations of Belonoshko *et al.*[5] (see Fig. 1). In reality, there is no experimental evidence that this melting curve exists. The fraction of local structures required to fit the melting measurements are plotted in Fig. 11. The fraction rises steadily to a maximum of $x=0.5$, at 150 GPa. At this pressure the fraction of local liquid structures is sufficiently large to create a solid-liquid mixed phase.

Frank[47] was the first to suggest that the surprising stability of undercooled metals against crystallization could be based on the packing of fivefold symmetric icosahedral units. In terms of Frank's idea the phase diagram of Mo can be viewed, in a broad sense, as one in which the bcc solid is in equilibrium with a pressure stabilized clustered melt. While the present model is not predictive, it is transparent, and connects the DAC and shock measurements, and introduces local structures into the phase diagram in a manner thermodynamically consistent and in the spirit of Frank's proposal.

V. DISCUSSION

The bcc-melting curve has now been reproduced by two independent sets of DAC measurements. First, made at the *Max-Planck Institut* in Mainz, by observing speckle motion in the melt and melt structures[2(a)] up to 90 GPa, and now by

X-ray diffraction measurements made at the ESRF in Grenoble extended to 119 GPa. The appearance of diffuse X-ray scattering, disappearance of diffraction peaks, and rapid recrystallization in the experiments provide strong evidence for melting, supporting a melting curve on Mo with a low slope. The experimental evidence is clear that there are no high temperature bcc to hcp or fcc transitions up to 119 GPa. The presence of such a transition would have been readily detected by the X-ray measurements. These data, and the Poisson ratios obtained from the sound speed data above 150 GPa in the shock experiments, are in disagreement with the proposed bcc-hcp shock transition at 210 GPa first proposed.[1] In terms of understanding the nature of the melt a free energy model suggests that the Mo melt is a complex structured liquid more akin to supercooled liquid phase than a simple liquid. Unfortunately, the X-ray diffraction data obtained in the present study are not suited to detect the presence of local structures in the melt. Local structures in transition metal liquids have been detected by neutron scattering,[36,37] and X-ray scattering techniques.[38] Theoretical studies, that focus on determining the microscopic local structure of the liquid melt[38–43] would be helpful in better understanding the phase diagram.

It should be obvious that the phase diagram of Mo possess many features that are unique and worthy of further investigation. The fact that unusually low melting slopes have also been found in the early transition metals Ta, W, Cr, Ti, V, and Y indicates that the present results are a general feature of the early transition metals and not confined to Mo. Mo is unique, only because it has been examined extensively by shockwave experiments. Ta, while less fully examined by shock experiments, appears to have many of the same features as Mo.[4] A more detailed understanding of the Mo phase diagram invites new shock measurements of the sound speeds between about 100 and 210 GPa. The necessary experimental facilities exist, and the expertise is available.

ACKNOWLEDGMENTS

The work by M.R. was performed under the auspices of the U.S. Department of Energy, by the Lawrence Livermore National Laboratory under Contract No. DE-AC52-07NA27344, and the Max-Planck-Institute für Chemie at Mainz, Germany. D.E. thanks the support of the Spanish MICINN (Grant No. CSD-2007-00045) and the Generalitat Valenciana (Projects No. GV2008-112).

[1] R. A. Hixson, D. A. Boness, J. W. Shaner, and J. A. Moriarty, Phys. Rev. Lett. **62**, 637 (1989).
[2] (a) D. Errandonea, B. Schwager, R. Ditz, R. Boehler, and M. Ross, Phys. Rev. B **63**, 132104 (2001); (b) D. Errandonea, R. Boehler, and M. Ross, Phys. Rev. Lett. **85**, 3444 (2000).
[3] M. Ross, R. Boehler, and D. Errandonea, Phys. Rev. B **76**, 184117 (2007).
[4] M. Ross, D. Errandonea, and R. Boehler, Phys. Rev. B **76**, 184118 (2007).
[5] A. B. Belonoshko, L. Burakovsky, S. P. Chen, B. Johansson, A. S. Mikhaylushkin, D. L. Preston, S. I. Simak, and D. C. Swift, Phys. Rev. Lett. **100**, 135701 (2008).
[6] C. Cazorla, M. J. Gillan, S. Taioli, and D. Alfè, J. Chem. Phys. **126**, 194502 (2007); C. Cazorla, D. Alfè, and M. J. Gillan, Phys. Rev. Lett. **101**, 049601 (2008).
[7] A. S. Mikhaylushkin, S. I. Simak, L. Burakovsky, S. P. Chen, B. Johansson, D. L. Preston, D. C. Swift, and A. B. Belonoshko, Phys. Rev. Lett. **101**, 049602 (2008).
[8] J. A. Moriarty, Phys. Rev. B **45**, 2004 (1992).
[9] R. Boehler, M. Ross, and D. B. Boercker, Phys. Rev. Lett. **78**, 4589 (1997).
[10] R. Boehler, M. Ross, and D. B. Boercker, Phys. Rev. B **53**, 556 (1996).
[11] R. Boehler and M. Ross, Earth Planet. Sci. Lett. **153**, 223 (1997).
[12] H. Brand, D. P. Dobson, L. Vocadlo, and I. G. Wood, High Press. Res. **26**, 185 (2006).
[13] S. Japel, B. Schwager, R. Boehler, and M. Ross, Phys. Rev. Lett. **95**, 167801 (2005).
[14] A. B. Belonoshko, R. Ahuja, O. Eriksson, and B. Johansson, Phys. Rev. B **61**, 3838 (2000).
[15] L. Vocadlo and D. Alfé, Phys. Rev. B **65**, 214105 (2002).
[16] L. Vocadlo, D. Alfé, G. D. Price, and M. J. Gillan, J. Chem. Phys. **120**, 2872 (2004).
[17] R. Boehler, Rev. Sci. Instrum. **77**, 115103 (2006).
[18] H. K. Mao, J. Xu, and P. M. Bell, J. Geophys. Res. **91**, 4673 (1986).
[19] S. Vennila, S. R. Kulkarni, S. K. Saxena, H. P. Liermann, and S. V. Sinogeikin, Appl. Phys. Lett. **89**, 261901 (2006).
[20] Y. Zhao, A. C. Lawson, J. Zhang, B. I. Bennett, and R. B. Von Dreele, Phys. Rev. B **62**, 8766 (2000).
[21] A. P. Jephcoat, R. J. Hemley, and H. K. Mao, Physica B **150**, 115 (1988).
[22] S. Ono, T. Kikegawa, and T. Iuzuka, Phys. Earth Planet. Inter. **145**, 9 (2004).
[23] R. Boehler, N. V. Bargen, and A. Chopelas, J. Geophys. Res., [Solid Earth Planets] **95**, 21731 (1990).
[24] A. Dewaele, M. Mezouar, N. Guignot, and P. Loubeyre, Phys. Rev. B **76**, 144106 (2007).
[25] R. Boehler, D. Santamaría-Pérez, D. Errandonea, and M. Mezouar, J. Phys.: Conf. Ser. **121**, 022018 (2008).
[26] G. Weck, P. Loubeyre, J. H. Eggert, M. Mezouar, and M. Hanfland, Phys. Rev. B **76**, 054121 (2007).
[27] A. Boultif and D. Louer, J. Appl. Crystallogr. **24**, 987 (1991).
[28] W. Kraus and G. Nolze, J. Appl. Crystallogr. **29**, 301 (1996).
[29] A. Chopelas and R. Boehler, Geophys. Res. Lett. **16**, 1347 (1989).
[30] G. Shen and P. Lazor, J. Geophys. Res. **100**, 17699 (1995).
[31] A. Zerr and R. Boehler, Science **262**, 553 (1993).
[32] J. Shaner, J. M. Brown, and R. G. McQueen, Mater. Res. Soc. Symp. Proc. **22**, 137 (1984).
[33] R. Boehler and M. Ross, Earth Planet. Sci. Lett. **153**, 223 (1997).
[34] J. A. Moriarty, D. A. Young, and M. Ross, Phys. Rev. B **30**, 578 (1984).
[35] C. Berne, A. Pasturel, M. Sluiter, and B. Vinet, Phys. Rev. Lett. **83**, 1621 (1999).
[36] T. Schenk, D. Holland-Moritz, V. Simonet, R. Bellissent, and D. M. Herlach, Phys. Rev. Lett. **89**, 075507 (2002).
[37] G. W. Lee, A. K. Gangopadhyay, K. F. Kelton, R. W. Hyers, T. J. Rathz, J. R. Rogers, and D. S. Robinson, Phys. Rev. Lett. **93**, 1982 (2004).
[38] T. H. Kim and K. F. Kelton, J. Chem. Phys. **126**, 054513 (2007).
[39] N. Jakse and A. Pasturel, J. Chem. Phys. **120**, 6124 (2004).
[40] N. Jakse and A. Pasturel, J. Chem. Phys. **123**, 244512 (2005).
[41] N. Jakse and A. Pasturel, Phys. Rev. Lett. **91**, 195501 (2003).
[42] N. Jakse, O. Le Bacq, and A. Pasturel, Phys. Rev. B **70**, 174203 (2004).
[43] B. Lee and G. W. Lee, J. Chem. Phys. **129**, 024711 (2008).
[44] M. Ross, L. H. Yang, and R. Boehler, Phys. Rev. B **70**, 184112 (2004).
[45] D. H. E. Dubin and H. DeWitt, Phys. Rev. B **49**, 3043 (1994).
[46] A. L. Ruoff, H. Xia, H. Luo, and Y. K. Vohra, Rev. Sci. Instrum. **61**, 3830 (1990).
[47] F. C. Frank, Proc. R. Soc. London, Ser. A **215**, 43 (1952).